DOI: 10.21062/mft.2023.049 http://www.journalmt.com

Microstructure, Mechanical Properties and Strengthening Mechanism of Back Extruded WE71 Magnesium Alloy Cylindrical Parts

Ting Li (0009-0007-3576-0754)[1,*] Dehao Bu (0000-0003-1531-8241)[2], Jiawei Yuan (0000-0003-2700-6229)[3], Xiaolei Han (0009-0005-9770-9431)[4], Zhiwei Du (0009-0000-7226-3916)[5], Zhaoqian Sun (0009-0005-4217-9621)[6], Yonggang Peng (0000-0003-4200-0802)[7], Kui Zhang (0000-0003-2051-9486)[8]
[1, 4, 5, 7]National Center of Analysis and Testing for Nonferrous Metals and Electronic Materials, GRINM Group Co., Ltd., Beijing 100088, China
[1, 4, 5, 7]Guobiao (Beijing) Testing & Certification Co., Ltd., China United Test & Certification Co., Ltd., Beijing 100088, China
[2]General Research Institute for Nonferrous Metals, Beijing 100088, China
[3, 6, 8]State Key Laboratory for Fabrication and Processing of Non-Ferrous Metals, GRIMAT Engineering Institute Co., Ltd., Beijing, 101407, China
[*]li20221123@163.com

In the present work, the microstructure, crystal orientation, mechanical properties and strengthening mechanisms for different areas of WE71 cylindrical parts have been investigated. The results show that from inner wall to outer wall, second phases density, DRX fraction decrease but average grain size increase, which is well agree with the strain state and metal flow during back extrusion. For compression area, <0001>$_\alpha$//ED texture type can be found in area a, but <0001>$_\alpha$ directions deflect from ED to TD at a certain angle for area b and c. For shear area, <0001>$_\alpha$ directions deflect from ED to TD about 10°~45°. For stable forming area, the texture is close to<10$\bar{1}$0>$_\alpha$//ND. After peak ageing, a large number of nanometer scaled β' phases have formed and uniformly distributed in the Mg matrix, while zigzag GP zone and RE-hexagons precipitates can also be found in the peak-aged alloy. Tensile properties for area c in compression area are the lowest: UTS, YS and EL are 322 MPa, 215 MPa and 2.5%, respectively. Furthermore, for the stable forming area, the UTS, YS and EL of 283 MPa, 187 MPa and 19% in the area f are the highest, but the strength of area g is the lowest, which is related to the grain size and volume fraction of second phases on flow lines. The strengthening contributes from fine-grain strengthening, texture strengthening and Orowan strengthening.

Keywords: magnesium alloy; back extrusion; strengthening mechanism; grain refinement

1 Introduction

Magnesium alloys play an increasingly important role in energy conservation and weight reduction due to their low density and high specific strength [1-3]. Especially, magnesium cylindrical parts have been widely used in many areas recent years, such as aerospace field and military industry. However, the manufacturing of Mg parts with complex shapes and high mechanical properties is difficult, owing to their hexagonal close-packed (HCP) crystallographic structure and insufficient slip systems. Thus, the poor workability is one of the factors that restrict the applications and development of Mg cylindrical parts [4-6].

As one of the useful forming method to manufacture Mg parts with complex shapes, back extrusion has been used for several decades [7-11]. Jiang et al. [12] proposes the use of truncated cone billets to prepare Mg alloy wheels by single-step back extrusion forming process based on streamline analysis. They found that for the magnesium alloy wheels formed by single-step back extrusion, truncated cone billets can increase the effective strain, dynamic recrystallize volume fraction and refine grains at the spokes and the lower rim, simultaneously improve the fluidity at the rim, making the rim filling easier and reducing the cracking tendency at the upper rim. Moreover, as a new method for the preparation of fine-grained microstructures, alternating back extrusion (ABE) has been reported for the processing of Mg cylindrical parts. Wang et al. [13] found that effective grain refinement can be achieved using accumulative alternating back extrusion, the mean grain size of ABE in one loading cycle decreased with the increase of downward loading depth of the split stem. After loaded in different directions in alternating back extrusion, the Schmid values both for basal slip system and pyramidal slip system showed a higher value, thus the pyramidal slip system was easier to open or lower the opening temperature, which was beneficial for the processing of Mg alloys with

complex shapes. Wang [14] established the ABE load theoretical model through the flow field simulated by the finite element method, slip line field distribution in cylindrical Mg parts was described. The results showed that affected by the maximum principal stress, the crystal orientation was segregated along with the stress distribution, and there was a preferred orientation in the microstructure that basal plane was related to the flow velocity field after alternating. Grain size was significantly refined via discontinuous dynamic recrystallization (DDRX) and uniformity increased with subsequent extrusion cycles. Asqardoust [15] applied the accumulative back extrusion to severely deform an as-extruded coarse grain Mg-4.35Y-3RE-0.36Zr alloy, and a significant improvement in both the strength (yield and ultimate) and elongation was obtained by the effects of grain size, the level of bimodality and the texture.

The deformation flow stress distribution, microstructure and mechanical properties of back-extruded parts have been extensively investigated in many reports as mentioned above. However, heterogeneity of microstructure, mechanical properties of back-extruded cylindrical parts due to inhomogeneous deformation, and their strengthening mechanism in detail has not been elaborated systematically. Thus, in the present work, the microstructure, crystal orientation, mechanical properties and strengthening mechanism for different positon of the cylindrical parts during back extrusion have been extensively investigated.

2 Material and Research Method

As extruded WE71 alloy with the chemical composition of Mg-7.44Y-0.84Nd-0.59Zr (wt. %) was used for the fabrication of cylindrical parts. Prior to back extrusion, the billets were preheated at 733 K for 2 h to enhance the deformability and reduce the risk of cracking. The extrusion rods with 25 mm in diameter was produced by back extrusion at 460 °C with an extrusion ratio of 24:1 and a ram speed of 0.4 $mm \cdot s^{-1}$. Finally, a high quality thick-walled cylindrical part with 190 mm in outer diameter, 130 mm in inner diameter, and 185 mm in height was prepared. After extrusion, some of the billets were aged at 200℃ for 38h to reveal the peak aged microstructure and mechanical properties.

The three-dimensional schematic of back extruded sample and sampling position is shown in Fig. 1. According to the stress state of cylindrical parts during back extrusion, three areas are marked as stable forming area, compression area and shear area respectively, as shown in Fig.1. In order to investigate the non-uniformity of microstructures, specimens for the microstructure observation are sampled as labeled in Fig.1. Three samples in compression area were taken from the inner wall to the outer wall labeled as a, b and c. Two samples in shear area were taken from the inner wall to the outer wall and labeled as area d and area e. Three samples in the stable forming area were taken from the inner wall to the outer wall along ED(extrusion direction), and labeled as area f, area g and area h, respectively. The tensile tests were carried out along the TD of area c, and the ED of area f, g and h, respectively.

Microstructure observations were performed through scanning electron microscopy (SEM) equipped with EDS and transmission electron microscopy (TEM). The surface of sample was mechanically ground with sandpapers and polished to mirror surface, then the microstructures were observed and analyzed by JSM-7900F microscopy. Disc samples (3 mm diameter) for TEM, HRTEM and HAADF-STEM analyses were ground to 60 μm thick and then twin-jet electro-polished in a solution of 5 vol.% perchloric acid and 95 vol.% ethanol, at temperature of 238 K and the voltage of 22 V, and then thinned by Gatan Precision Ion Polishing System at 173 K for about 20min. The microstructures were observed and analyzed by Talos F200X. The mechanical properties of these alloys were evaluated by tensile testing cylindrical samples with 5mm diameter and 25mm gauge length. Tensile tests were conducted using the SANS tensile testing machine at a speed of 2 $mm \cdot min^{-1}$at room temperature.

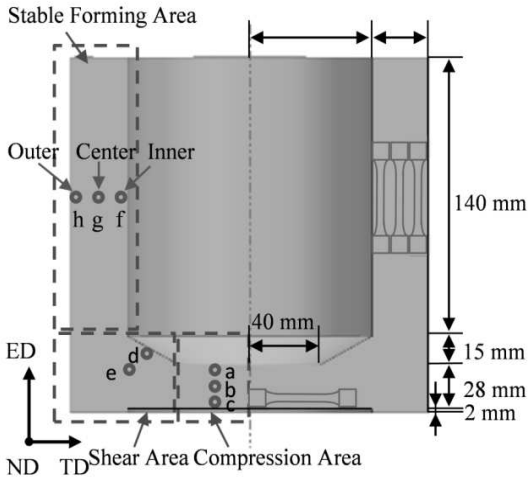

Fig. 1 *The three-dimensional schematic and sampling diagram of back extruded cylindrical samples*

3 Results and discussions

3.1 Microstructure of as-extruded samples

The SEM microstructures for area a-h of cylindrical part are shown in Fig. 2. It can be seen that masses of second phases with different directions have formed during the back extrusion. For area a, b and c that in compression area, orientations of second

phases onflow lines are consistent with the direction of metal flow which are distributed at a certain angle with the TD due to the compression deformation. For area d and e, 45º degree that between TD and the directions of flow lines can be found which is consistentwith the metal flow in shear area. Similarly, for area h, g and f in stable forming area, 90º degree between TD and the directions of flow lines can be found. In addition, larger quantity of second phases in inner wall (area f, d and a) can be seen which may be attributed to the larger stress in these areas contacted with stem during back extrusion. These phases were identified to be Mg_5RE phase with f.c.c(a=2.13nm), Y-rich phase with f.c.c(a=0.52nm) and Zr-rich particles by TEM and EDS analysis that have been published elsewhere.

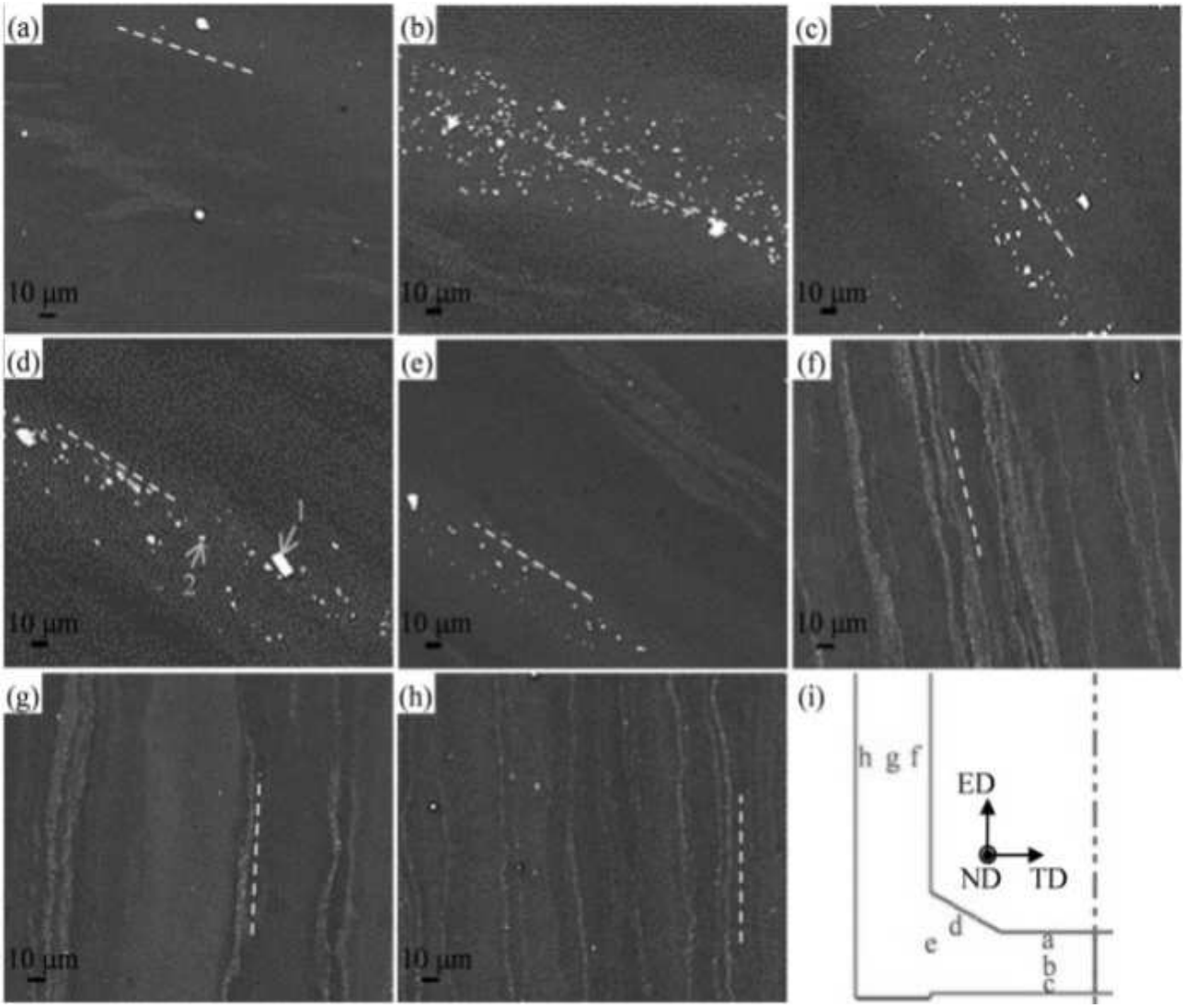

Fig. 2 *(a-h) SEM images of the cylindrical part corresponding to area a-h; (i) schematic of the samples*

Fig. 3 shows the inverse pole figures(IPF) maps, image quantity+grain orientation spread (IQ+GOS) maps and grain size distribution maps for the samples a,b and c of compression area. For area c as shown in Fig.3g and h, partly dynamic recrystallization can be found that fine DRX grains formed around the second phases and grain boundaries of the deformed grains, showing a heterogeneous chain-likely distribution. Due to the poor mobility of metal and lower strain during back extrusion in the dead zone, the DRX fraction is relatively low that of 32.2%, and the fraction for coarse deformed grains with grain size larger than 35 μm is about 42.05%. As shown in Fig.3i, the average grain size for area c is about 30.5 μm. Forareab as shown in Fig.3 d, e and f, DRX fraction of 85.2% is higher than that of area c. The average grain size is about 14.6 μm. In this area, the coarse deformed grains with grain size larger than 35 μm decreased to 3.68%. For area a, a completely recrystallized microstructure with DRX fraction of 94.6% can be found. The average grain size for area a is about 11.5μm. From inner wall (area a) to outer wall (area c), DRX fraction decreased but average grain size increased gradually. It can be concluded that the microstructure evolution is identified with the strain state and metal flow in compression area, the lower grain size and larger DRX fraction is corresponding to the larger effective strain than area c in dead zone.

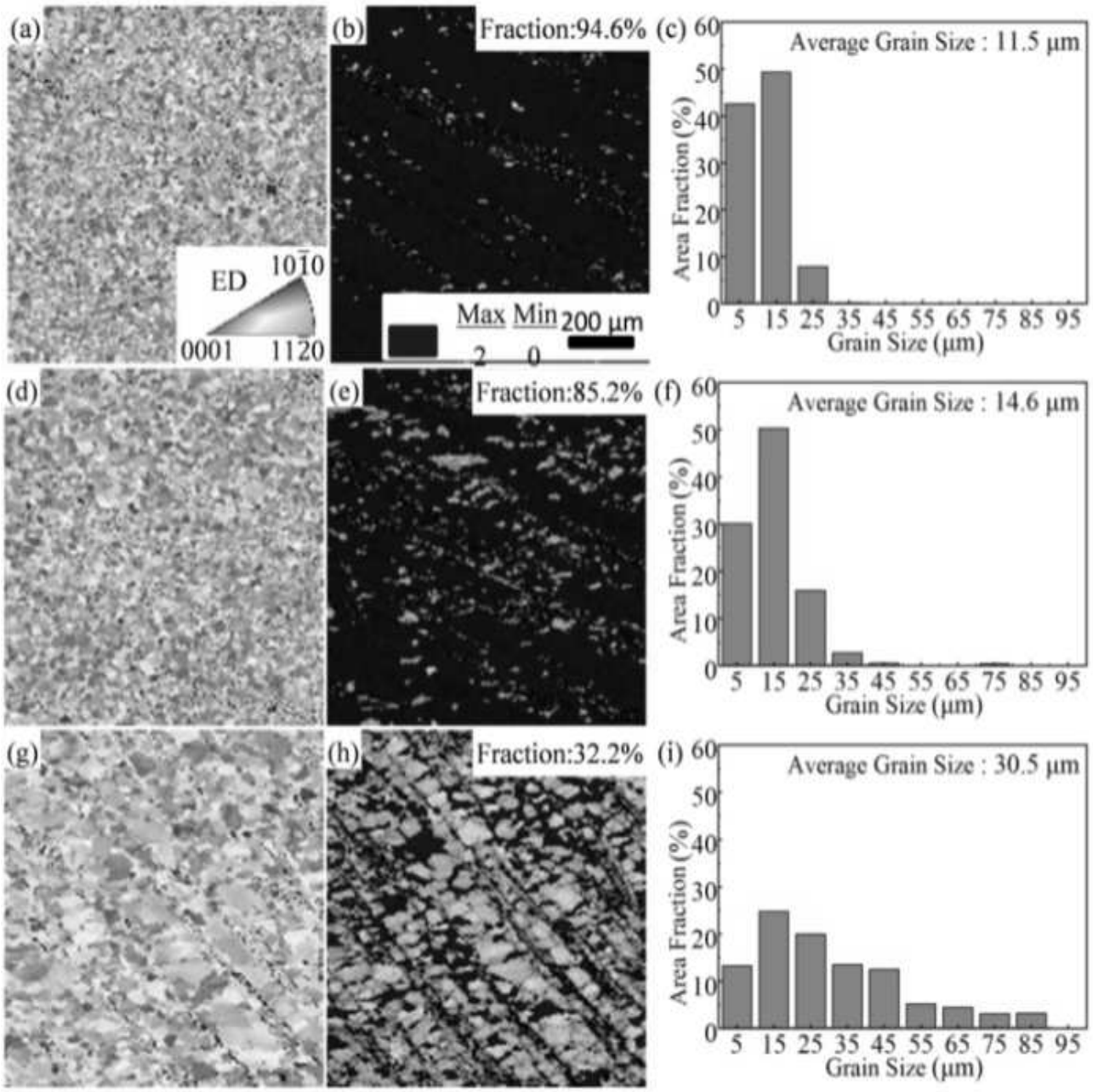

Fig. 3 *EBSD images for compression area (a-c) area a; (d-f) area b; (g-i) area c; (a,d,g) IPF map; (b,e,h) IQ+GOS map; (c,f,i) grain size distribution map*

TheEBSD analysis results for areas d and e of shear area is shown in Fig.4. As seen in Fig. 4, the IPF and IQ+GOS maps are almost consisted of completely equiaxed recrystallized grains. The DRX fractions and average grain size for areas d and e are 95.7%, 11.3 μm, and 86.2%, 14.2 μm, respectively. It can also be seen that the fraction of grains with larger than 30 μm size in area e is significantly reduced after shear deformation. On the other side, the fraction of grains with grain size larger than 30 μm for area d is smaller, but area fraction of grains with grain size less than 10 μm increases to about 45%, which maybe attributed to the larger effective strain during extrusion.

Fig. 5 shows the EBSD analysis results for areas f, g and h of stable forming area. From IPF and IQ+GOS maps, it can be seen that the DRX fraction decrease from 97.9% of inner wall(area f) to 88.8% of outer wall(area h). However, the grain size distribution maps indicate that the average grain size is 13.1, 16.8, and 11.6μm for area f, g and h, respectively. The relatively smaller grain size of area h is ascribed to the higher fraction of grains with grain size less than 10μm.This is because the more homogenous flow lines composed of second phases as seen in Fig. 5g-h, which can effectively hinder the growth of DRX grains. In addition, the ununiform microstructure of the initial WE71 bars that the average grain size of center is much larger than that of the edge maybe the other reason.

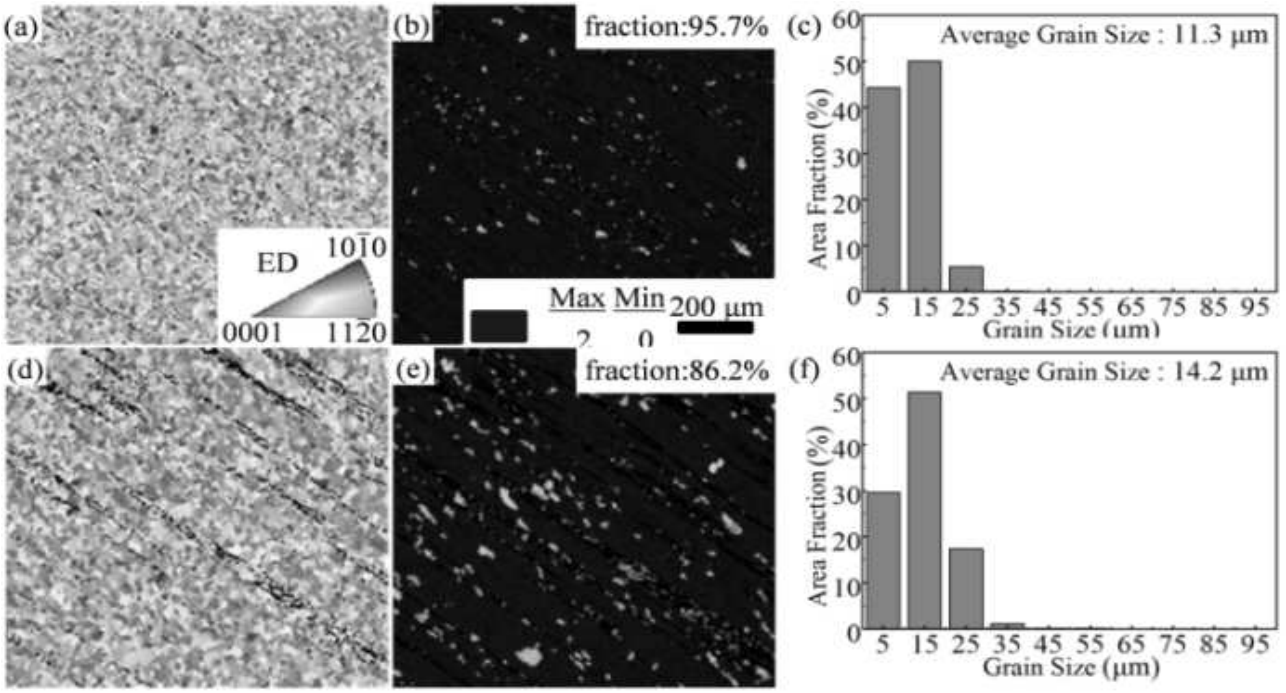

Fig. 4 *EBSD images for shear area (a,b,c) area d; (d,e,f) area e; (a,d) IPF map; (b,e) IQ+GOS map; (c,f) grain size distribution map*

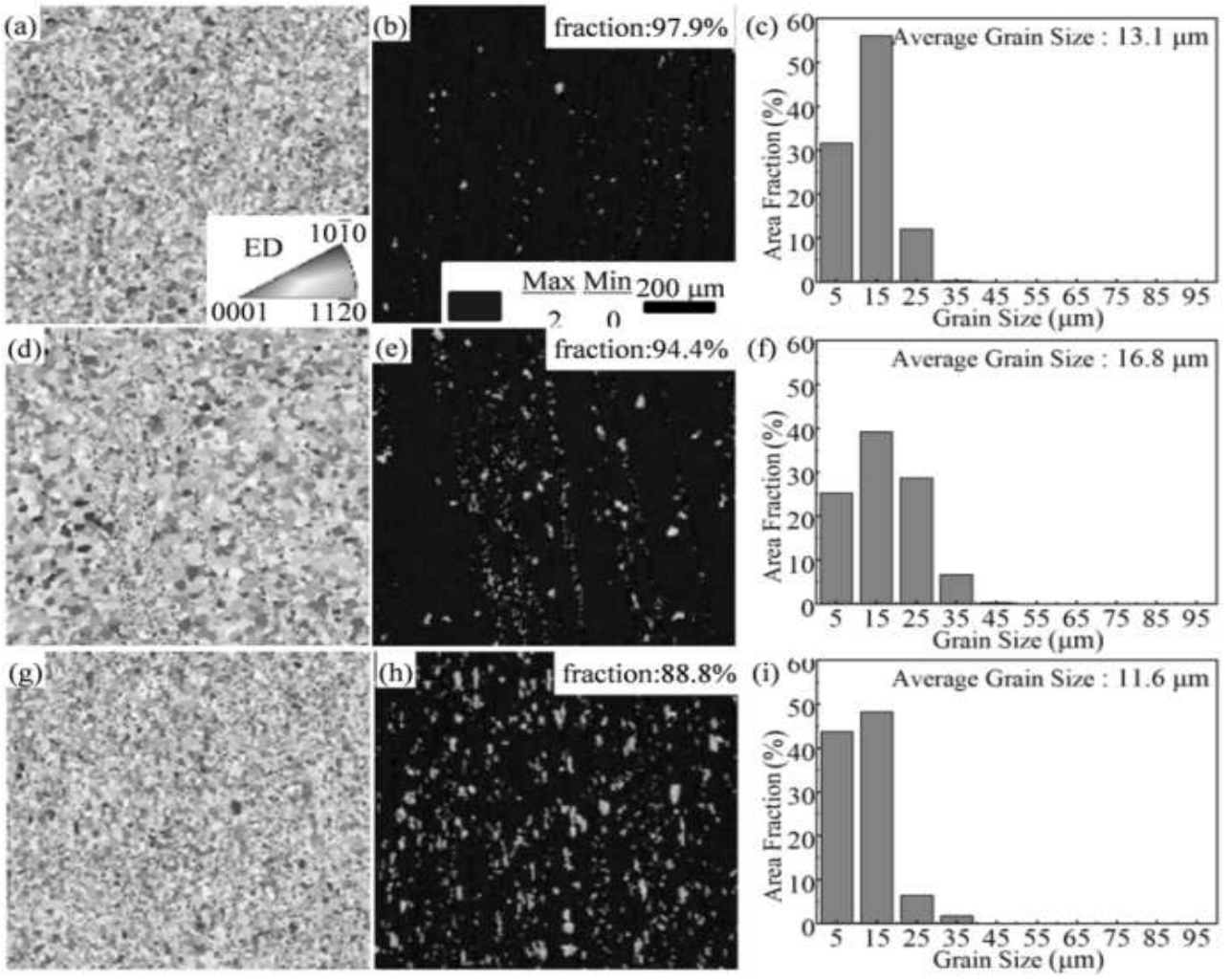

Fig. 5 *EBSD images for stable forming area (a-c) areaf; (d-f) area g; (g-i) area h; (a,d,g) IPF map; (b,e,h) IQ+GOS map; (c,f,i) grain size distribution map*

To reveal the micro-texture evolution during the back extrusion process, the pole figures (PF) and inverse pole figures (IPF) of all the samples are shown in Fig. 6. For area in compression area, $<0001>_\alpha$//ED texture with maximum pole intensity (MPI) of 2.767 can be found, in which $(0001)_\alpha$ base plane is perpendicular to the extrusion direction, and there is still a preferred orientation of $<10\bar{1}0>_\alpha$//ND and $<2\bar{1}\bar{1}0>_\alpha$. However, $<0001>_\alpha$ directions deflects from ED to TD at a certain angle for area b and c, and intensity of $<10\bar{1}0>_\alpha$//ND component decreased simultaneity. For shear area, $<0001>_\alpha$ directions deflects from ED to TD about 10°~45° with the MPI of 3.672 in area e. For stable forming area, the texture is close to$<10\bar{1}0>_\alpha$//ND, that is $(0001)_\alpha$ base plane is parallel to the extrusion direction.

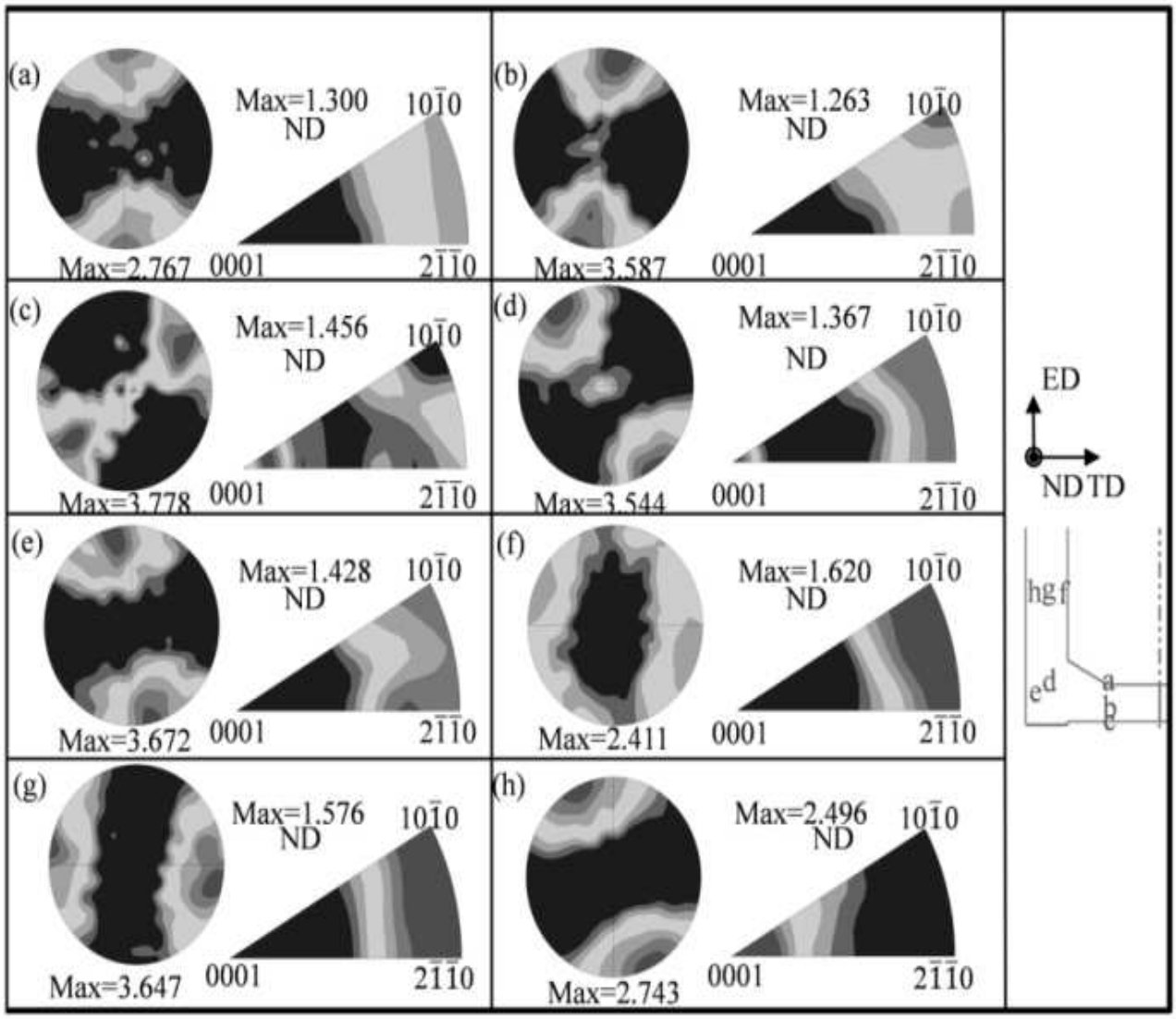

Fig. 6 *(a-h)Pole figures and inverse pole figures for area a-h*

3.2 Microstructure of as-aged samples

To reveal the microstructure of peak-aged samples, Fig.7 shows the HAADF-STEM image and corresponding SAED patterns of area h aged at 240°C for 200h. Viewing from [0001]α zone axis, a typical microstructure feature of β' phase that formed on the $\{11\bar{2}0\}_\alpha$ planes with three variants can be found. Viewing from $[11\bar{2}0]_\alpha$, all the β' precipitates are arranged in the same direction that is parallel to $[0001]_\alpha$. The precipitates have a plate-shape with approximately 3-14 nm length along $[0001]_\alpha$, 1-8nm length along $[10\bar{1}0]_\alpha$ and 3-10nm length along $[11\bar{2}0]_\alpha$. The overlapped SAED pattern indexed according to b.c.o. structure with a = 0.64 nm, b = 2.22 nm and c = 0.52 nm also indicate the precipitation of β' phases in WE71 alloy. Besides, zigzag GP zone and RE-hexagons precipitates can also be found in the peak-aged alloy.

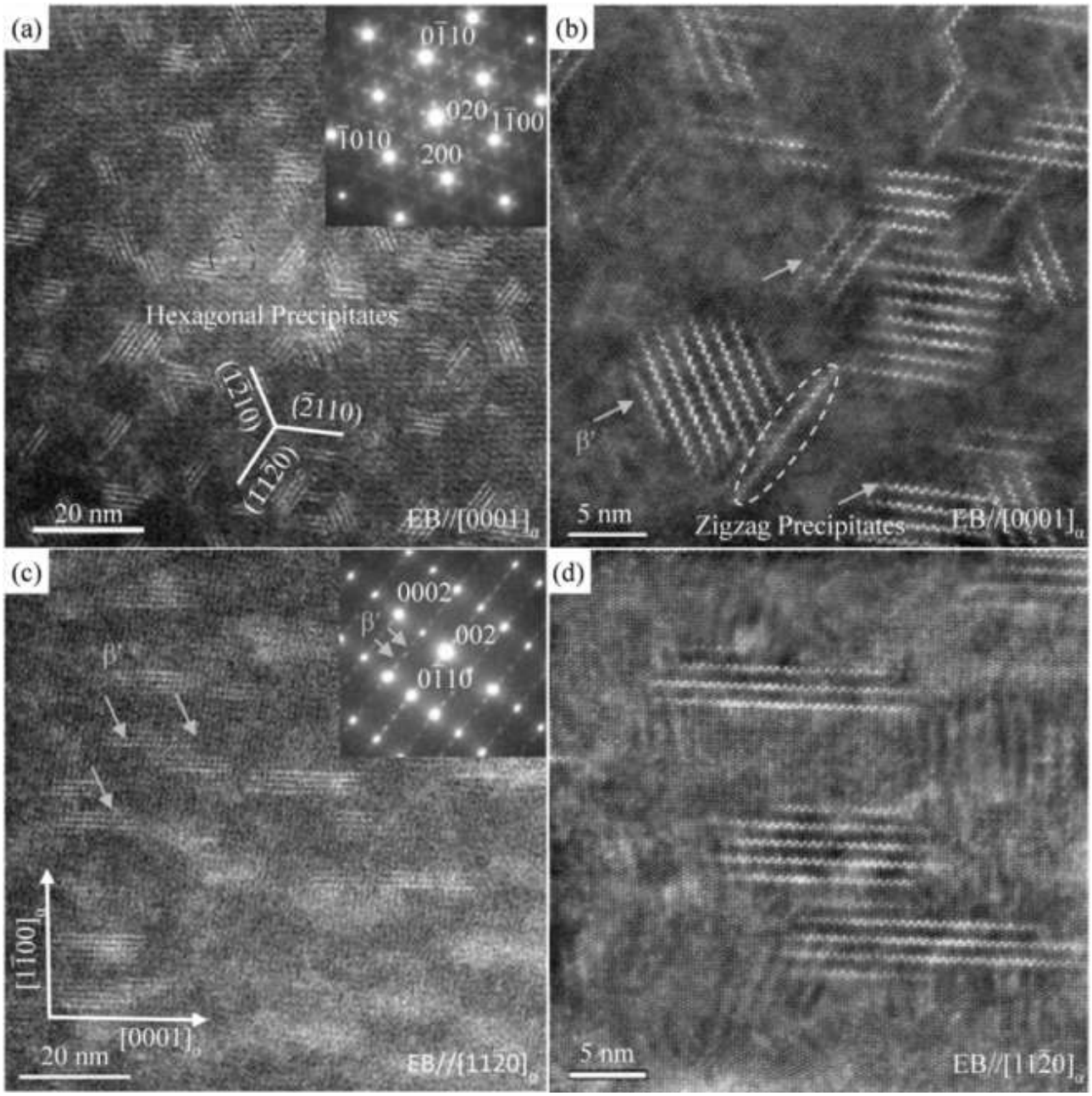

Fig. 7 *Microstructures of samples from area h aged at 240 °C for 38h (a,b) HAADF-STEM image and corresponding FFT pattern taken along$[0001]_\alpha$; (c,d) HAADF-STEM image and corresponding FFT pattern taken along$[11\bar{2}0]_\alpha$*

3.3 Mechanical properties

The tensile properties of samples from compression area and stable forming area are shown in Fig. 8. It can be seen that the tensile properties for area c in compression area are the lowest: ultimate tensile strength (UTS), yield strength (YS) and elongation (EL) are 322 MPa, 215 MPa and 2.5%, respectively. Furthermore, for the stable forming area, the UTS, YS and EL of 283 MPa, 187 MPa and 19% in the area f are the highest, but the strength of area g is the lowest, which is related to the grain size results that illustrated above. Thus, the fine-grain strengthening is one of the significant strengthening mechanisms.

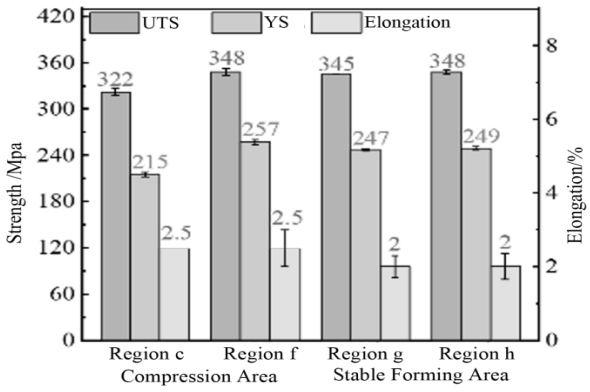

Fig. 8 *Ultimate tensile strength, yield strength, and elongation for different areas of the as-aged cylindrical parts*

3.4 Strengthening mechanism

Based on the microstructure analysis above, three mainstrengthening mechanisms can be concluded as: (1) fine-grainstrengthening, due to grain-boundaries blocking dislocations; (2) texture strengthening, due to the strong preferential orientation of grains; (3) Orowan strengthening due to the interaction of dislocations with fine particles consist of second phases distributed on flow lines and precipitates formed during ageing heat treatment. The increments of the three strengthening mechanisms at different positions of the cylindrical parts are investigated as follows:

Grian refinement strengthening is one of the most significant ways to improve the yield strength of magnesium alloys, the effect of grain size on the yield strength can be described as Hall-Petch formula [16]:

$$\Delta\sigma_{\mathrm{H-P}} = Kd^{-1/2} \quad (1)$$

where $\Delta\sigma_{\mathrm{H-P}}$ is the increment of grain refinement strengthening on yield strength, k is the influence coefficient of grain boundary on deformation, which is mostly between 200~300 MPa·μm$^{-1/2}$ for magnesium alloys, and k=250 MPa·μm$^{-1/2}$ will be taken for calculation, d is the average grain size, μm. Take the average grain size of 30.5μm, 13.1μm, 16.8μm and 11.6μm described above to the calculation of Eq.1 for areas c, f, g and h, respectively. Thus, the strength increment caused by grain boundaries can be calculated to be 45.27, 69, 61 and 73.4 for areas c, f, g and h, respectively. The same variation tendency can be found between the total strength and grain refinement strengthening increment for area c and h in outer wall, suggest that the fine grain strengthening is the dominant strengthening mechanisms.

Texturestrengthening is important in extruded Mg alloy due to the preferential orientation of grains. When the tensile direction is parallel to the $\{0001\}_\alpha$ basal plane, the base plane slip is difficult to start and the YS is higher. When the $\{0001\}_\alpha$ base plane and tensile direction are 45°, the grains show soft orientations and the YS decreases. For area c, f, g and h, although the different orientation can be found in Fig. 5, but the tensile directions are all almost parallel to $\{0001\}_\alpha$ basal planes. Besides, due to the high RE content in WE71 alloy and sufficient dynamic recrystallization, the average Schmid factors of basal slip for areas c, f, g and h are 0.32, 032, 0.30, and 0.32, respectively, which are close to each other that texture strengthening for the strength difference in the present research can be negligible.

Orowan strengthening is attributed to the interactions between dislocations and particles including second phases distributed on flow lines and precipitates formed during ageing, and is given by the Orowan-Ashby equation, where M is orientation factor(6.5)[17], G is shear modulus of Mg-Matrix (17.3GPa)[18], b is Burger's vector of Mg-matrix (3.21×10^{-10}m), dp is average size of reinforcing particles, visPossion's ratio (0.35)[19-20], V_p is volume fraction of the reinforcing particles:

$$\Delta\sigma_{\mathrm{Orowan}} = \frac{0.4MGb}{\pi\sqrt{\frac{2}{3}}d_p\sqrt{1-\nu}\sqrt{\frac{\pi}{4V_p}-1}}\ln\left(\sqrt{\frac{2}{3}}\frac{d_p}{b}\right) \quad (2)$$

Due to the same ageing heat treatment, the volume fraction and average size of precipitates are nearly the same for different areas of cylindrical part, thus the Orowan strengthening of second phases on flow lines will be focused to explain the strength deviation for area f, g and h. As mentioned above, the type and size of second phases for different areas is similarly, but the larger volume fraction in inner wall (area f) compared with outer wall (area h) is obvious attributed to the larger stress in these areas contacted with stem during back extrusion. As a result, the contribution of Orowan strengthening of second phases can be calculated as 15.5 and 7.6 MPa for areas f and h respectively, thus the calculated strength difference that combined Orowan strengthening and grain refinement strengthening is very close to the total yield strength deviation [21-22].

4 Conclusions

The microstructure, crystal orientations, mechanical properties and strengthening mechanisms for different areas of the WE71 cylindrical parts during back extrusion have been investigated. The results are concluded as follows:

- 1) The type and size of second phases for different areas are similarly, but the larger volume fraction of second phases in inner wall compared with that in outer wall is obvious attributed to the larger stress in these areas contacted with stem during back extrusion.
- 2) DRX fractions decrease but average grain sizes increase gradually from inner wall to outer wall, which is identified with the strain state and metal flow. The smaller grain size and larger DRX fraction are corresponding to the larger effective strain.
- 3) For compression area, $<0001>_\alpha$//ED texture type can be found, but $<0001>_\alpha$ directions deflect from ED to TD at a certain angle for area b and c. For shear area, $<0001>_\alpha$ directions deflect from ED to TD about 10°~45. For stable forming area, the texture is close to$<10\bar{1}0>_\alpha$//ND.

- 4) Fine-grain strengthening and Orowan strengthening of phases consist of second phases distributed on flow lines and precipitates formed during ageing heat treatment are the main strengthening mechanisms for WE71 cylindrical parts.

Acknowledgement

This study was supported by the Natural Science Foundation of China (No. 51501015 and No. 51871195), and the Science and Technology Project of Henan Province (Project Nos. 222102230113).

References

[1] ZHANG, J.H., LIU, S.J., WU, R.Z., HOU, L., ZHANG, M.L. (2018). Recent developments in high-strength Mg-RE-based alloys: Focusing on Mg-Gd and Mg-Y systems. *Journal of Magnesium and Alloys*, 6(3): 277-291. https://doi.org/10.1016/j.jma.2018.08.001

[2] YOU, S.H., HUANG, Y.D., KAINER, K.U., HORT, N. (2017). Recent research and developments on wrought magnesium alloys. *Journal of Magnesium and Alloys*, 5(3): 239-253. https://doi.org/10.1016/j.jma.2017.09.001

[3] BIAN, M.Z., NAKATSUGAWA, L., MATSUOKA, Y., HUANG, X.S., TSUKADA, Y., KOYAMA, T., CHINO, Y.(2022). Improving the mechanical and corrosion properties of pure magnesium by parts-per-million-level alloying plastic deformation. *ActaMaterialia*, 241: 118393. https://doi.org/10.1016/j.actamat.2022.118393

[4] XIA, Q.X., LONG, J.C., XIAO, G.F., YUAN, S., QIN, Y. (2021). Deformation mechanism of ZK61 magnesium alloy cylindrical parts with longitudinal inner ribs during hot backward flow forming. *Journal of Materials Processing Technology*, 296: 117197. https://doi.org/10.1016/j.jmatprotec.2021.117197

[5] CHALAY-AMOLY, A., ZAREI-HANZAKI, A., CHANGIZIAN, P., FATEMI-VARZANEH, S.M., MAGHSOUDI, M.H. (2013). An investigation into the microstructure/strain pattern relationship in backward extruded AZ91 magnesium alloy. *Materials & Design*, 47: 820-827. https://doi.org/10.1016/j.matdes.2013.01.006

[6] CHE, X., WANG, Q., DONG, B.B., MENG, M., GAO, Z., LIU, K., MA, J., YANG, F.L., ZHANG, Z.M. (2021). The evolution of microstructure and texture of AZ80 Mg alloy cup-shaped pieces processed by rotating backward extrusion. *Journal of Magnesium and Alloys*, 9(5): 1677-1691. https://doi.org/10.1016/j.jma.2020.07.013

[7] FATEMI-VARZANEH, S.M., ZAREI-HANZAKI, A. (2009). Accumulative back extrusion (ABE) processing as a novel bulk deformation method. *Materials Science and Engineering: A*, 504(1-2): 104-106. https://doi.org/10.1016/j.msea.2008.10.027

[8] FARAJI, G., JAFARZADEH, H., JEONG, H.J., MASHHADI, M.M., KIM, H.S. (2012). Numerical and experimental investigation of the deformation behavior during the accumulative back extrusion of an AZ91 magnesium alloy. *Materials & Design*, 35: 251-258. https://doi.org/10.1016/j.matdes.2011.09.057

[9] SHATERMASHHADI, V., MANAFI, B., ABRINIA, K., FARAJI, G., SANEI, M. (2014). Development of a novel method for the backward extrusion. *Materials & Design (1980-2015)*, 62: 361-366. https://doi.org/10.1016/j.matdes.2014.05.022

[10] HOSSEINI, S.H., ABRINIA, K., FARAJI, G. (2015). Applicability of a modified backward extrusion process on commercially pure aluminum. *Materials & Design (1980-2015)*, 65: 521-528. https://doi.org/10.1016/j.matdes.2014.09.043

[11] MENG, Y.Z., YU, J.M., ZHANG, G.S., WU, Y.J., ZHANG, Z.M., SHI, Z. (2020). Effect of circumferential strain rate on dynamic recrystallization and texture of Mg-13Gd-4Y-2Zn-0.5Zr alloy during rotary backward extrusion. *Journal of Magnesium and Alloys*, 8(4): 1228-1237. https://doi.org/10.1016/j.jma.2019.12.012

[12] JIANG, Y.C., ZHU, Y.T., LE, Q.C., LIAO, Q.Y., ZHOU, W.Y., WANG, P., WANG. T. (2022). Effect of truncated cone billet on single-step back extrusion forming process of magnesium alloy wheel. *Journal of Materials Research and Technology*, 20: 1533-1543. https://doi.org/10.1016/j.jmrt.2022.07.117.

[13] WANG, Y., LI, F., HUO, P.D., LI, C., GUAN, X.R. (2022). Correlation between stress state and crystal orientation distribution in alternating back extrusion of magnesium alloy. *Mechanics of Materials*, 173: 104416. https://doi.org/10.1016/j.mechmat.2022.104416.

[14] WANG, Y., LI, F., BIAN, N., XIAO, X.M. (2021). Coordinated control of preferred orientation and uniformity of AZ31 in accumulative alternating back extrusion. *Materials Science & Engineering A*, 818: 141366. https://doi.org/10.1016/j.msea.2021.141366.

[15] ASQARDOUST, S., ZAREIHANZAKI, A., ABEDI, H.R., KRAJNAK, T., MINÁRIK, P. (2017). Enhancing the strength and ductility in accumulative back extruded WE43 magnesium alloy through achieving bimodal grain size distribution and texture weakening. *Materials Science and Engineering: A*,698: 218-229.https://doi.org/10.1016/j.msea.2017.04.098

[16] CHEN, Z.H. (2005). Wrought magnesium alloy [M]. Chemical Industry Press.

[17] HAN, B.Q., DUNAND, D.C. (2000). Microstructure and mechanical properties of magnesium containing high volume fractions of yttriadispersoids. *Materials Science and Engineering: A*, 277(1-2): 297-304. https://doi.org/10.1016/S0921-5093(99)00074-X.

[18] LI, X., STAMPFL, J., PRINZ, F.(2000). Mechanical and thermal expansion behavior of laser deposited metal matrix composites of Invar and TiC. *Materials Science and Engineering: A*,282 (1-2): 86-90. https://doi.org/10.1016/S0921-5093(99)00781-9.

[19] MONDET, M., BARRAUD, E., LEMONNIER, S., GUYON, J., ALLAIN, N., GROSDIDIER, T. (2016). Microstructure and mechanical properties of AZ91 magnesium alloy developed by Spark Plasma Sintering. *Acta Materilia*,119: 55-67. https://doi.org/10.1016/j.actamat.2016.

[20] PRŮCHA, V., JANSA, Z., & VESELÝ, V. (2021). Influence of Deep Cryogenic Processing on Carbide Grain Size in Sintered Car-bide WC-Co. *Manufacturing Technology*, 21(1): 117-123. DOI: 10.21062/mft.2021.004

[21] BRADÁČ, J, SOBOTKA, J. (2023). Evaluation of Riveting Force Influence on the Quality of Riveted Joint of Aluminium Alloy EN AW - 6016. *Manufacturing Technology*, 23(1): 2-10. Doi: 10.21062/mft.2023.011

[22] ŠKOLÁKOVÁ, A, LOVAŠI, T, PINC, J, KAČENKA, Z, RIESZOVÁ, L, ŽOFKOVÁ, Z. (2020). The Effect of Zinc and Calcium Addition on Magnesium Alloy. *Manufacturing Technology*, 20(5): 668-676. Doi: 10.21062/mft.2020.107